Biomaterials 141 (2017) 125–135

Contents lists available at ScienceDirect

Biomaterials

journal homepage: www.elsevier.com/locate/biomaterials

Decoupling the effects of stiffness and fiber density on cellular behaviors via an interpenetrating network of gelatin-methacrylate and collagen

Anthony J. Berger [a], Kelsey M. Linsmeier [a], Pamela K. Kreeger [a, b, c, **], Kristyn S. Masters [a, c, d, e, *]

[a] Department of Biomedical Engineering, University of Wisconsin-Madison, Madison, WI, United States
[b] Department of Cell and Regenerative Biology, University of Wisconsin School of Medicine and Public Health, Madison, WI, United States
[c] Carbone Cancer Center, University of Wisconsin School of Medicine and Public Health, Madison, WI, United States
[d] Department of Medicine, University of Wisconsin School of Medicine and Public Health, Madison, WI, United States
[e] Department of Materials Science and Engineering, University of Wisconsin-Madison, Madison, WI, United States

ARTICLE INFO

Article history:
Received 20 May 2017
Received in revised form
26 June 2017
Accepted 28 June 2017
Available online 29 June 2017

Keywords:
Collagen
Stiffness
Tumor microenvironment
Fibers

ABSTRACT

The extracellular microenvironment provides critical cues that guide tissue development, homeostasis, and pathology. Deciphering the individual roles of these cues in tissue function necessitates the development of physically tunable culture platforms, but current approaches to create such materials have produced scaffolds that either exhibit a limited mechanical range or are unable to recapitulate the fibrous nature of *in vivo* tissues. Here we report a novel interpenetrating network (IPN) of gelatin-methacrylate (gelMA) and collagen I that enables independent tuning of fiber density and scaffold stiffness across a physiologically-relevant range of shear moduli (2–12 kPa), while maintaining constant extracellular matrix content. This biomaterial system was applied to examine how changes in the physical microenvironment affect cell types associated with the tumor microenvironment. By increasing fiber density while maintaining constant stiffness, we found that MDA-MB-231 breast tumor cells required the presence of fibers to invade the surrounding matrix, while endothelial cells (ECs) did not. Meanwhile, increasing IPN stiffness independently of fiber content yielded decreased invasion and sprouting for both MDA-MB-231 cells and ECs. These results highlight the importance of decoupling features of the microenvironment to uncover their individual effects on cell behavior, in addition to demonstrating that individual cell types within a tissue may be differentially affected by the same changes in physical features. The mechanical range and fibrous nature of this tunable biomaterial platform enable mimicry of a wide variety of tissues, and may yield more precise identification of targets which may be exploited to develop interventions to control tissue function.

1. Introduction

Alterations to extracellular matrix (ECM) stiffness and density occur during tissue aging [1] and disease [2–5] and have the potential to impact cell behavior within the tissue. For example, numerous *in vitro* studies have shown that substrate rigidity can influence the organization and generation of intracellular forces [6], overall cell morphology [7,8], and intracellular signaling [9,10], thereby affecting the differentiation of stem cells [11], migration of a variety of cell types [12–14], and invasiveness of cancer cells [15]. While much of this research has been performed on 2D substrates, most cell types *in vivo* are physically supported by a 3D fibrous ECM, the density and structure of which provide contact guidance cues that are important in cell morphology and invasion [16–18]. However, independently examining the function of fibrous ECM stiffness and density in order to determine their individual roles in cellular processes in 3D is a non-trivial pursuit.

* Corresponding author. 1111 Highland Ave, 8531 WIMR II Madison, WI 53705, United States.
** Corresponding author. 1111 Highland Ave, 4553 WIMR II Madison, WI 53705, United States.
E-mail addresses: kreeger@wisc.edu (P.K. Kreeger), kmasters@wisc.edu (K.S. Masters).

http://dx.doi.org/10.1016/j.biomaterials.2017.06.039
0142-9612/

Reconstituted ECM molecules are often used to create 3D environments for *in vitro* studies due to their ability to mimic the natural bioactivity of physiological environments. Such materials are frequently exploited to study stiffness-dependent effects, as increases in ECM density result in reduced fiber flexibility, leading to an increase in the elastic modulus [19,20]. However, this approach does not allow matrix rigidity to be modulated independently of the concentration of bioactive ECM ligands or ECM density. Additionally, both Matrigel and collagen I form gels primarily via non-covalent interactions [21,22], resulting in mechanically weak structures. As most biological tissues are viscoelastic scaffolds with elastic moduli that vary across tissue types (*e.g.,* 0.1 kPa for brain, 100 kPa for soft cartilage) [23], and pathological conditions such as breast cancer progression can alter the compressive moduli within a single tissue from 0.4 to 10 kPa [24], these current methods are able to replicate only a narrow window of physiologically or pathophysiologically relevant mechanics. Chemical modifications to the ECM, commonly through collagen glycation [25] or crosslinking [26,27], can be used to increase scaffold rigidity, but these techniques yield only slight increases in the achievable range of stiffnesses and often present new complications, such as prolonged incubations, the introduction of new bioactive ligands, and/or alterations to the ECM architecture.

Gelatin-methacrylate (gelMA) has recently emerged as an attractive option for creating engineered ECM-based matrices that possess a wide range of physical properties while maintaining constant gelatin concentration [28]. However, while gelatin is identical in protein composition to collagen, it cannot assemble into triple helices, and thereby does not allow the formation of the higher order fibrillar structures exhibited by collagen *in vivo*. Purely synthetic hydrogels, such as polyethylene glycol diacrylate (PEGDA) scaffolds, can also allow independent manipulation of ligand density and matrix stiffness over a wide range of mechanical properties [29,30], but, similar to gelatin, lack the ability to recapitulate the fibrous networks of *in vivo* tissues. This limitation is problematic because fibers may play important roles in directing cell behavior; for example, fibrillar alignment of collagen in breast tumors has been shown to correlate with a worse patient prognosis [31,32]. The influence of fibrillar structure on cellular outcomes was also highlighted by recent work which described a significant decrease in mouse xenograft tumor growth upon attenuation of fiber formation and crosslinking by inhibition of LOXL2 [33]. Here, we report a novel method for fabricating an interpenetrating network (IPN) hydrogel of gelMA and collagen I which allows for a wide variation of shear modulus while retaining the fibrillar structure of collagen. Furthermore, by varying the ratio of gelMA to collagen, this approach also permits manipulation of matrix fiber density without changing the overall protein content. Using this approach to decouple fiber density and scaffold stiffness, we investigated how these individual physical cues influence cell behavior in the context of the tumor microenvironment. Specifically, we quantified the invasion of MDA-MB-231 breast cancer cells, as changes in tissue stiffness and collagen architecture are prominent features of breast cancer progression. Additionally, as angiogenesis is a key process that supports tumor progression [34], we examined the impact of these cues on endothelial cell sprouting to determine how these responses varied for different cell types that may be present within the same pathophysiology.

2. Materials and methods

2.1. Materials and cell culture

Unless otherwise noted, all chemicals were purchased from Sigma-Aldrich (St. Louis, MO). MDA-MB-231 human breast cancer cells (ATCC, Manassas, VA) and bovine aortic endothelial cells (BAECS, Cell Applications, San Diego, CA) were used until passage 25 and 9, respectively. Cells were maintained at 37 °C and 5% CO_2 in DMEM (Invitrogen, Carlsbad, CA) supplemented with 10% Hyclone fetal bovine serum (Thermo Scientific, Logan, UT), 100 U/mL penicillin-streptomycin, and 2 mM L-glutamine.

2.2. Gelatin methacrylation

GelMA was synthesized using a modification of a previously published procedure [35]. Briefly, type-A porcine skin gelatin was dissolved at 10% w/v in phosphate buffered saline (PBS) at 50 °C. While both type A and type B gelatin can be methacrylated, gelMA synthesized with type A is more common in the field and better characterized. Methacrylic anhydride (MA) was added to the gelatin solution using a peristaltic pump at a rate of 200 μL/min under aggressive stirring. Final MA concentrations of 0.25, 2.5, and 7% v/v were used and will be referred to as 0.25 M, 2.5 M, and 7 M herein. The reaction proceeded for 24 h at 50 °C shielded from light. The solution was spun down at 3000 × g for 5 min to pellet unreacted MA and precipitated protein. The supernatant was dialyzed against PBS using 12–14 kDa MWCO dialysis tubing (Spectrum Labs, Rancho Dominguez, CA) for 2 days at 50 °C, at which point the dialysis solution was switched to ddH_2O for another 3 days at 50 °C. Dialysis buffer was changed daily during dialysis. The gelMA solution was filtered, lyophilized, and stored at −20 °C.

2.3. Hydrogel formation and optimization

To generate hydrogels, gelMA was first resuspended at 20% w/v in PBS and incubated in a 50 °C water bath until dissolved. The 0.25 M, 2.5 M, and 7 M gelMA solutions were blended in varied ratios to tune the gel mechanical properties, with the goal of producing three different gel stiffness conditions. The gelMA solution was then combined with the photoinitiator lithium phenyl-2,4,6-trimethylbenzoylphosphinate (LAP; 0.05% w/v final concentration) [36], PBS, and collagen (or equivalent amount of gelatin) in a 37 °C water bath. The prepolymer solution was then incubated at 37 °C for 30 min to polymerize the collagen, at which point the gelMA was photocrosslinked via UV exposure at 365 nm (3.4 mW/cm^2) for 5 min at 37 °C (Fig. 1A). The swelling of the gels was measured as percent increase in wet weight after a 24 h incubation at 37 °C in PBS, and an iterative process was followed to modify the starting prepolymer formulations in order to achieve a final, post-swelling concentration of 5% gelMA across all conditions. Briefly, the initial gelMA concentration was adjusted to accommodate gel volume changes that occurred during swelling, and the final gel formulations used 5.5–7.4% initial gelMA concentrations to yield a final gelMA concentration of 5% across all conditions.

Within each stiffness condition, varied amounts of bovine skin collagen (Fibricol – a 10 mg/mL solution of native bovine type I Collagen, Advanced Biomatrix, San Diego, CA), were added to produce gelMA-collagen gels. Fibricol was added to a solution containing gelMA, PBS, and LAP, and the mixture was briefly vortexed and centrifuged, neutralized with 10X PBS and 0.1 M sodium hydroxide, vortexed and centrifuged again, and then crosslinked as described above. This process was used to generate gels at each stiffness containing a final concentration of 0, 1.5, or 3 mg/mL collagen (Fig. 1B). To maintain constant total protein concentration across all conditions, gels that included 0 or 1.5 mg/mL collagen were supplemented with unmodified gelatin to yield a final amount of 3 mg/mL added protein (i.e., no collagen + 3 mg/mL gelatin; 1.5 mg/mL collagen + 1.5 mg/mL gelatin; or 3 mg/mL collagen + no gelatin). The addition of fibrous collagen increases the stiffness of the resulting hydrogel. To compensate for this, an

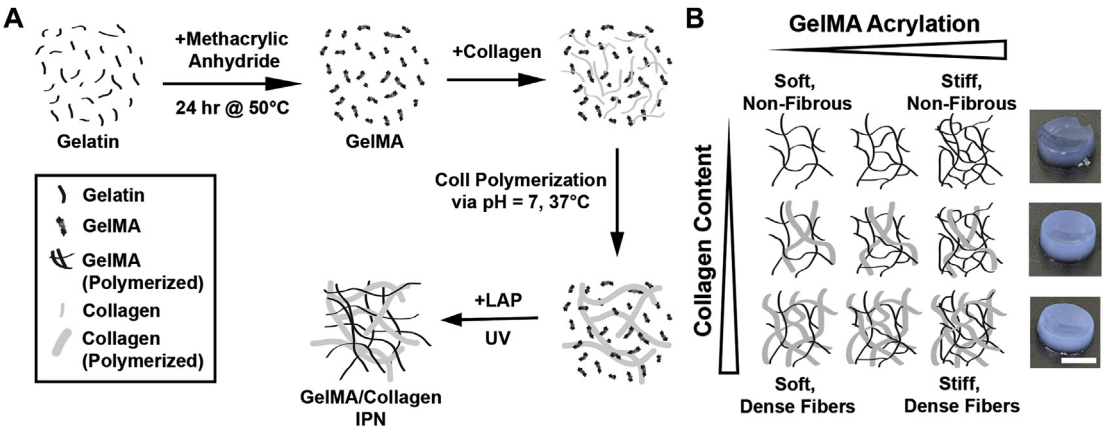

Fig. 1. An interpenetrating network of collagen and gelMA was formed to allow for independent tuning of scaffold stiffness and collagen fiber content. (A) Collagen was polymerized in the presence of gelMA, which was then crosslinked via UV exposure in the presence of the photoinitiator LAP. (B) By changing the amount of collagen and the degree of gelMA methacrylation, the fiber content and scaffold stiffness can be tuned. Hydrogel images depict 7 kPa with 0, 1.5, or 3 mg/mL collagen (top to bottom), scale bar = 5 mm.

iterative process was used to maintain constant stiffness of the scaffolds upon addition of different amounts of collagen or unmodified gelatin by adjusting the average degree of gelMA acrylation in the starting formulation. Example formulations for 1 mL prepolymer of each condition are listed in Supplementary Table 1.

2.4. Quantification of total protein content in GelMA/Collagen hydrogels

After determining the appropriate starting gelMA concentration, the total protein content of GelMA/Collagen hydrogels was quantified via measurement of free amines using a ninhydrin assay after acid digestion. Hydrogels were fabricated as described above and polymerized as discs in a 4 mm × 1.5 mm silicone mold. The gels were allowed to swell in PBS overnight at 37 °C. To solubilize the scaffolds, gels were incubated in a 1:4 volume of 7 N H_2SO_4 for 18 h at 105 °C. After cooling to room temperature, the digested scaffolds were diluted in ddH_2O and mixed with ninhydrin reagent. Samples were boiled for 10 min, allowed to cool, diluted 1:2 with 95% ethanol, and the absorbance was measured at 570 nm on a Tecan Infinity M1000 plate reader (Tecan, San Jose, CA). Unmodified gelatin solution was digested and prepared alongside gelMA/collagen samples in order to generate the standard curve in the ninhydrin assay.

2.5. Evaluation of hydrogel elastic moduli

Hydrogels were fabricated as discs in an 8 mm × 1.5 mm silicone mold. The discs were swelled in PBS at 37 °C overnight, and rheometry was performed to determine elastic moduli (ARES rheometer, TA Instruments, New Castle, DE). Dynamic strain tests were performed at 37 °C with constant frequency (0.1 Hz) and oscillating strain. Gels were glued [37] with Loctite Super Glue Gel (Loctite, Westlake, Ohio) to 8 mm parallel plates and allowed to set for 5 min before initiating the measurement. The shear storage modulus was determined from the linear viscoelastic region. Dynamic frequency sweeps, with constant strain (the value being determined by the viscoelastic region of the dynamic strain tests) and oscillating frequency showed 0.1 Hz to be within the stable linear region for all conditions.

2.6. Collagen organization in GelMA/Collagen hydrogels

Fluorescent staining of collagen fibers was used to qualitatively examine collagen distribution within the different GelMA/Collagen hydrogels. The prepolymer was pipetted into a 96 well plate (75 μL per well), polymerized, and swollen in PBS overnight. The gels were incubated in 5 μM collagen-binding adhesion protein 35 fused with enhanced green fluorescent protein (CNA35-EGFP) for 18 h at 37 °C. The CNA35-EGFP, a fluorescently tagged collagen-binding protein that preferentially labels fibrillar collagen, was expressed and purified from *E. coli* as previously described [38]. The pET28a-EGFP-CNA35 plasmid was a gift from Maarten Merkx (Addgene plasmid # 61603). Following incubation, gels were thoroughly rinsed with PBS via four 2-h washes at 37 °C, and then imaged on a Leica SP8 confocal microscope (Leica, Buffalo Grove, IL).

2.7. GelMA/collagen hydrogel degradation

Two different approaches were used to examine degradation of gelMA/collagen gels: measurement of collagen stability over the course of the experiments described herein, and degradation upon exposure to exogenously-added collagenase. To assess the stability of the collagen network under experimental conditions, collagen fibers within gelMA/collagen gels were imaged using CNA35-EGFP as described above, following a 72 h incubation in DMEM at 37 °C, 5% CO_2. To assess degradation upon exposure to exogenous collagenase, gelMA/collagen prepolymer solution was pipetted into a 96 well plate (75 μL per well), polymerized, and allowed to swell overnight at 37 °C in PBS. The buffer was then replaced with PBS containing 20 μg/mL collagenase type II (Worthington Biochemical, Lakewood, NJ). Samples of the supernatant were taken at 60, 120, 240, 360, and 480 min, and degradation was monitored via absorbance at 280 nm (NanoDrop 1000, Thermo Fisher Scientific, Waltham, MA). After 24 h, an endpoint measurement was taken of completely digested gels to normalize the earlier absorbance readings.

2.8. BAEC viability and morphology in gelMA/collagen gels

BAEC cultures were trypsinized to generate a single-cell suspension and diluted in gelMA/collagen prepolymer solution to 500,000 cells/mL. Hydrogel polymerization was conducted in a 96 well plate as outlined above (75 μL per well), after which gels were fed with serum-free DMEM supplemented with 25 ng/mL vascular endothelial growth factor (VEGF-165, Peprotech, Rocky Hill, NJ) and incubated at 37 °C and 5% CO_2. Cell viability was examined at 24 and 48 h post-encapsulation by incubating gels (n = 3 per

condition) with 2 μM calcein and 2 μM ethidium homodimer-1 (Invitrogen) in serum free DMEM for 30 min, washing with serum-free DMEM, and then imaged on a Leica SP8 confocal microscope. Images were converted to binary and the 'analyze particles' tool in FIJI [39] was utilized to count the number of fluorescent cells in the green and red channels. To calculate percent viability, the number of calcein positive cells was divided by the total number of cells.

Cell morphology within gelMA/collagen gels was examined at 24 h post-encapsulation. BAECs were fixed and permeabilized via incubation with 10% formalin for 10 min followed by another 10-min incubation with PBS +0.1% Triton X-100. Gels were then incubated in 5 μM CNA35-EGFP for 18 h at 37 °C. After four 2-h washes with PBS at 37 °C, intracellular actin and cell nuclei were stained with Alexa Fluor 564 phalloidin (0.165 μM, Invitrogen) and DAPI (0.3 μM), respectively, in PBS with 1% BSA. Gels were washed in PBS and imaged on a Leica SP8 confocal microscope. Cell length and width were measured using the FIJI 'Measure' tool, and aspect ratio was calculated by dividing the larger dimension by the smaller.

2.9. MDA-MB-231 morphology in gelMA/collagen gels

MDA-MB-231 cultures were trypsinized to generate a single-cell suspension and diluted in gelMA/collagen prepolymer to 500,000 cells/mL. Hydrogel polymerization was conducted as outlined above, after which gels were fed with serum-free DMEM supplemented with 25 ng/mL TGF-α (Peprotech). At 24 h post-encapsulation, MDA-MB-231 cells were fixed and permeabilized via incubation with 10% formalin for 10 min followed by another 10-min incubation with PBS +0.1% Triton X-100. Staining for collagen, actin, and cell nuclei was performed as described in the previous section.

2.10. MDA-MB-231 proliferation in gelMA/collagen gels

Proliferation of MDA-MB-231 cells within gelMA/collagen gels was determined using a Click-iT Edu imaging assay (Invitrogen) according to the manufacturer's instructions. Briefly, MDA-MB-231 cultures were trypsinized to generate a single-cell suspension and diluted in gelMA/collagen prepolymer to 1×10^6 cells/mL. Hydrogel polymerization in a 96-well plate was conducted as outlined above, after which gels were fed with serum-free DMEM supplemented with 25 ng/mL TGF-α. At 24 h post-encapsulation, EdU was spiked into the media, and cells were incubated for an additional 5 h, followed by fixation and permeabilization. AlexaFluor 488 azide was added to visualize proliferating cells while DAPI was used as a nuclear counterstain. Cells were imaged on a Leica SP8 confocal microscope and percent proliferating cells was determined by dividing the number of AlexaFluor 488 positive cells by the total number of cells.

2.11. BAEC spheroid fabrication

BAEC cultures were trypsinized to generate a single-cell suspension and diluted to 40,000 cells/mL in prewarmed growth medium supplemented with 0.2% methylcellulose. Drops of this cell suspension (30 μL) were then added to the inside of a plastic petri dish lid. The lid was inverted and placed over a petri dish filled with PBS. The cell droplets were incubated at 37 °C and 5% CO_2 in a humidified incubator for 24 h, yielding spheroids with an average diameter of 150–200 μm.

2.12. Tumor spheroid fabrication

MDA-MB-231 cell cultures were trypsinized to generate a single-cell suspension and diluted to 200,000 cells/mL in ice-cold growth medium. A volume of 50 μL was then added to each well of a 96-well v-bottom plate (Corning, Corning, NY). To prevent cell attachment, the plate was previously coated with 50 μL/well 1% Poly-HEMA in 95% ethanol and air dried at 37 °C for 3 days. The cells were pelleted into the v-bottom of each well by centrifugation at 1000 × g for 10 min at 4 °C using an Eppendorf 5810R centrifuge (Eppendorf, New York, NY). After centrifugation, 50 μL of ice cold growth medium supplemented with 10% Matrigel (BD Biosciences, San Jose, CA) was gently layered over each well. The plate was then incubated under standard culture conditions for 2 days, yielding spheroids with an average diameter of 250–300 μm.

2.13. Spheroid invasion assay in gelMA/collagen hydrogels

BAEC and tumor spheroids were collected, washed with serum-free DMEM, centrifuged at 500 × g, and resuspended in serum-free DMEM. The spheroid solution was then placed on a rotating platform and incubated at 37 °C for 20 min to remove any residual FBS and Matrigel (for tumor spheroid preparation) from the spheroids. This process was repeated 3 times.

The spheroid solution was combined with gelMA/collagen prepolymer to yield a final concentration of 1 spheroid/50 μL of hydrogel solution. The solution was distributed into a 96-well plate at 75 μL per well, and hydrogel polymerization was performed as described above. Gels were then fed with serum-free DMEM supplemented with either 25 ng/mL VEGF or TGF-α for BAEC or MDA-MB-231 spheroids, respectively. The gels were refed with serum-free DMEM containing 25 ng/mL VEGF or TGF-α every 24 h after embedding. At 72 h, spheroids were stained with 2 μM calcein-AM in serum-free media for 30 min, washed with serum free media, and imaged on an Olympus IX51 microscope (Olympus, Center Valley, PA). Image analysis was done with FIJI [39]. For BAEC spheroids ($n = 8–15$) images were skeletonized [40] and the length of all sprouts >5 μm in length was summed to quantify total sprout length. To quantify invasion area in tumor spheroids ($n = 6–9$) the images were converted to a binary display and the 'analyze particle' tool was used to determine the total area of cells (spheroid core + invading cells). The fold-change in cell-occupied area was calculated by dividing total area by the area of the spheroid core.

2.14. Statistics

Data were analyzed using one-way analysis of variance (ANOVA) and Tukey's test in Prism 7 (GraphPad Software, La Jolla, CA) with $p < 0.05$ considered statistically significant. All values are expressed as the mean ± standard deviation.

3. Results

3.1. A range of ECM stiffnesses and densities can be achieved with gelMA/collagen hydrogels

GelMA possessing varying degrees of methacrylation has previously been used to generate scaffolds with tunable mechanical properties [28]. To introduce a fibrous component to this system, collagen I was polymerized in the presence of uncrosslinked gelMA, which was then photopolymerized around the existing collagen architecture (Fig. 1A). Matrix stiffness was changed via alterations to the methacrylation degree of gelMA, while collagen fiber density was manipulated by changing the ratio of collagen I to unmodified gelatin (Fig. 1B). To investigate how the presence of fibers and

changes in scaffold stiffness affect cell behavior, gels with three different shear moduli (2, 7, and 12 kPa) and three different collagen concentrations at each shear modulus (0, 1.5, and 3 mg/mL) were fabricated. The composition of the gelMA/collagen prepolymer solution was adjusted to enable tuning of fibrillar collagen content in the absence of changes to elastic modulus (Fig. 2A), and to maintain equivalent total ECM content across all conditions (Fig. 2B).

3.2. Collagen I maintains fibrillar structure in GelMA/Collagen gels

To confirm the presence of a fibrillar collagen network within gelMA/collagen scaffolds, gels were stained with EGFP-tagged CNA35, a small protein that preferentially binds to fibrillar collagen [38]. Fluorescent visualization of the EGFP tag demonstrated a homogenous distribution of randomly oriented fibers in all collagen-containing conditions (Fig. 2C). Quantification of the percent area of the image that stained positively for collagen demonstrated a significant difference in collagen fiber density between the 1.5 mg/mL and 3 mg/mL conditions, as expected (Fig. 2D), and samples without added collagen did not produce a quantifiable signal. Changes in gel stiffness did not affect the percent area of collagen in either the 1.5 or 3 mg/mL condition. Additionally, there was no change in the percent area of collagen after a 72 h incubation in culture conditions (Supplemental Fig. 1), demonstrating the stability of the fibrous network under experimental conditions. Hydrogel degradation was also examined upon treatment with exogenous collagenase. Consistent with previous studies of gelMA alone [28], the rate of hydrogel degradation decreased as stiffness increased (Supplemental Fig. 2A), but degradation was unaffected by the addition of fibrillar collagen (Supplemental Fig. 2B).

3.3. Embedded cells are viable and able to interact with the gelMA/collagen scaffold

To ensure the materials and polymerization conditions were not cytotoxic, BAECs were embedded in the various gelMA/collagen scaffolds and stained with calcein AM/ethidium homodimer-1. At 48 h post-encapsulation, over 95% of BAECs were viable across all gelMA/collagen conditions (Fig. 2E). Viability at 24 h was similar (data not shown). Additionally, there was no significant difference in viability for BAECs embedded in gelMA/collagen scaffolds and a 3 mg/mL collagen-only gel at either time point ($p > 0.05$).

To visualize the morphology of BAECs and MDA-MB-231 cells within the material, Alexa Fluor 564 phalloidin, DAPI, and EGFP-CNA35 were used to stain actin, cell nuclei, and collagen architecture, respectively. Actin staining for both cell types appeared as puncta in gelMA gels with and without collagen fibers, suggesting the formation of focal adhesions by the cells within the material (Fig. 3). Furthermore, in the presence of 3 mg/mL collagen, cells were surrounded by a fibrous matrix, with cell protrusions that appeared to interact with collagen fibers and exhibited high levels of actin. In scaffolds containing only gelMA, no fibrillar structures or evidence of contact guidance were observed. BAECs were elongated and fibroblastic in both 0 and 3 mg/mL collagen conditions and exhibited similar aspect ratios (Fig. 3A and B) while MDA-MB-231 cells did not appear to develop protrusions and exhibited a significantly lower aspect ratio when collagen was not present (Fig. 3C and D). In addition, the proliferation of MDA-MB-231 cells increased upon the addition of collagen in the softest condition (2 kPa), but the magnitude of this change decreased with increasing stiffness (Supplemental Fig. 3).

3.4. Sprouting from BAEC spheroids is affected by both collagen content and matrix stiffness

To investigate how collagen fiber density and matrix stiffness independently affect endothelial cell behavior, BAECs were formed into spheroids and embedded in gelMA/collagen gels. Assessment of EC spheroid sprouting, a process that involves invasion in tandem with the development of vessel-like structures in the surrounding matrix, is often used as a means for evaluating angiogenic potential [41]. At 72 h following embedding, viable cells within the spheroids were fluorescently stained with calcein AM (Fig. 4A), and the total length of all EC sprouts emerging from each spheroid was quantified. Examination of the effect of increasing collagen density at each stiffness revealed that the presence of collagen in the softest (2 kPa) and stiffest (12 kPa) scaffolds significantly increased EC sprouting, although no concentration-dependent effect was observed. Meanwhile, cells in 7 kPa exhibited a differential response to collagen, where sprouting at 0 and 1.5 mg/mL was similar, and a slight decrease in sprout length occurred with the addition of 3 mg/mL collagen to the gelMA hydrogels (Fig. 4B). Examination of the effect of increasing stiffness at each collagen density revealed a gradual decrease in sprouting with increased stiffness for both 1.5 and 3 mg/mL collagen conditions (Fig. 4C). When no collagen was present, sprouting peaked at 7 kPa, but was reduced to near-zero in the 12 kPa condition.

3.5. MDA-MB-231 spheroids require collagen for invasion

Spheroids formed with MDA-MB-231 cells were also embedded in gelMA/collagen gels. Quantifying tumor spheroid invasion into a surrounding 3D matrix is a common method of evaluating metastatic potential [42]. At 72 h post-embedding, the spheroids were fluorescently labeled with calcein AM (Fig. 5A), and the fold change in cell invasion area relative to the area of the spheroid core was quantified. Examination of the effect of increasing collagen density at each stiffness revealed that, across all stiffnesses, the addition of collagen was necessary for invasion to occur, although there was no concentration-dependent effect (Fig. 5B). Evaluation of the influence of increasing stiffness at each collagen density demonstrated a sharp decrease as the scaffold rigidity moved from 2 to 7 kPa for both 1.5 and 3 mg/mL collagen conditions (Fig. 5C). Invasion was not significantly affected by further increasing matrix stiffness from 7 to 12 kPa.

4. Discussion

We have developed a novel method for fabricating ECM-based hydrogels that incorporates a fibrillar collagen structure, yielding materials that allow for independent tuning of scaffold stiffness and collagen fiber density while controlling for total ligand density. Generating *in vitro* systems capable of independently modulating microenvironmental properties will enable better understanding of cellular behaviors across a wide range of tissues and pathologies. Our initial studies of endothelial and tumor cell spheroids embedded within these scaffolds demonstrate the utility of our system in examining the impact of independently-varied microenvironmental cues on cell function. Notably, we found that increasing scaffold stiffness generally stimulates the opposite trend in cell sprouting/invasion compared to increasing collagen fiber density, an observation that could not be obtained using existing scaffold systems. We also demonstrate that the response to the presence of fibrillar collagen varies with cell type, a finding with implications for understanding the often-contradictory responses that can occur within multicellular tissues.

As noted above, the most common method for changing the

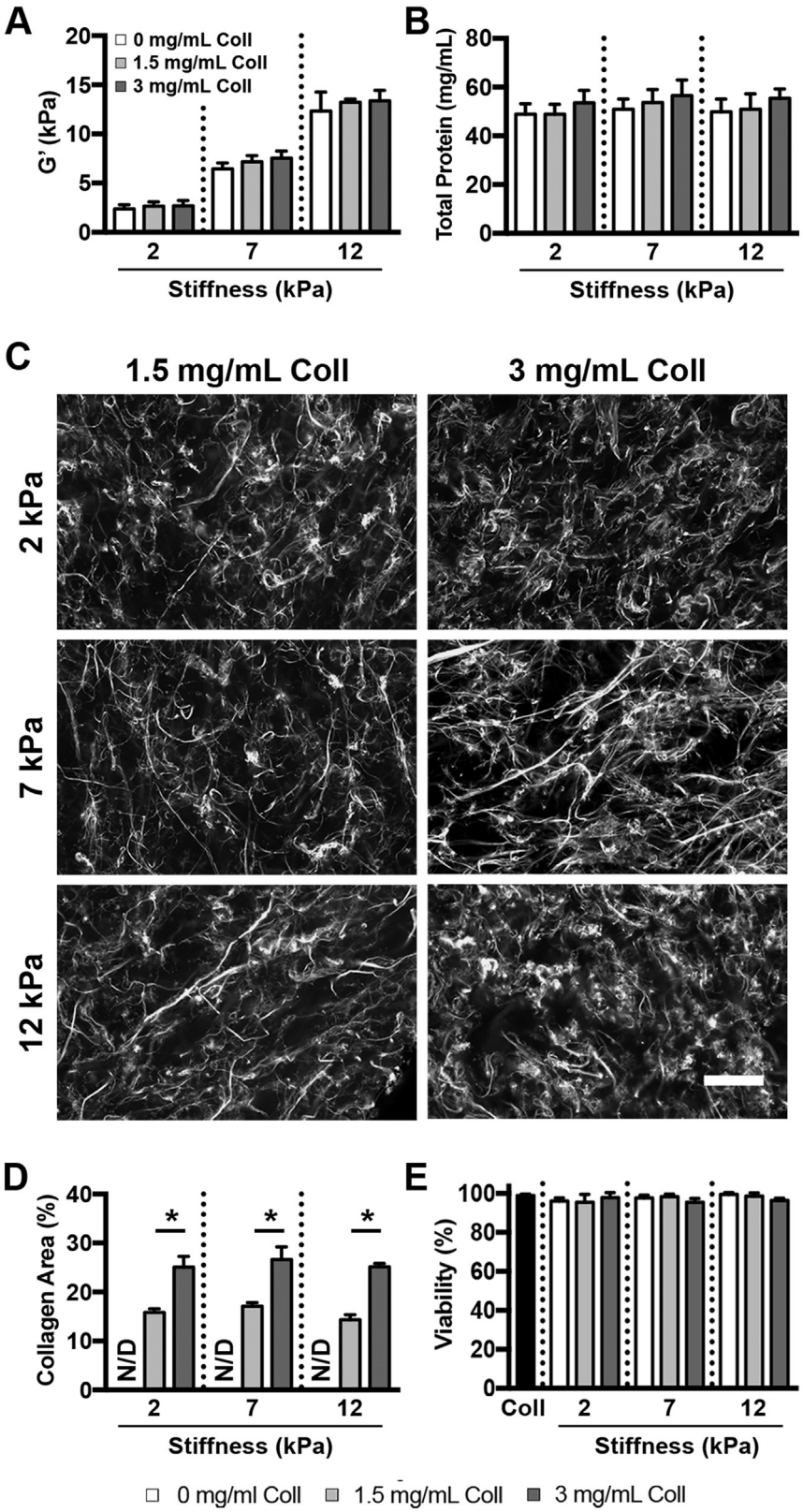

Fig. 2. Scaffold stiffness and collagen content can be independently tuned in gelMA/collagen gels. (A) GelMA/collagen hydrogels were fabricated at 3 stiffnesses (2, 7, and 12 kPa) and collagen content was varied from 0 to 3 mg/mL, n = 3 (B) Despite variations in collagen content and matrix rigidity, the total protein content was not significantly different across the gel conditions ($p > 0.05$), n = 3 (C) CNA35-EGFP labeling of gelMA/collagen hydrogels revealed a randomly oriented, fibrous network of collagen. Scale bar = 100 μm. (D) The area occupied by fluorescent fibrillar collagen increased with increasing collagen content and was not significantly affected by changes in scaffold stiffness. * indicates $p < 0.05$. N/D indicates not detectable, n = 3 (E) BAEC viability in gelMA/collagen gels was similar to collagen-only gels (Coll) at 48 h post embedding ($p > 0.05$), n = 3. Data represent mean ± standard deviation.

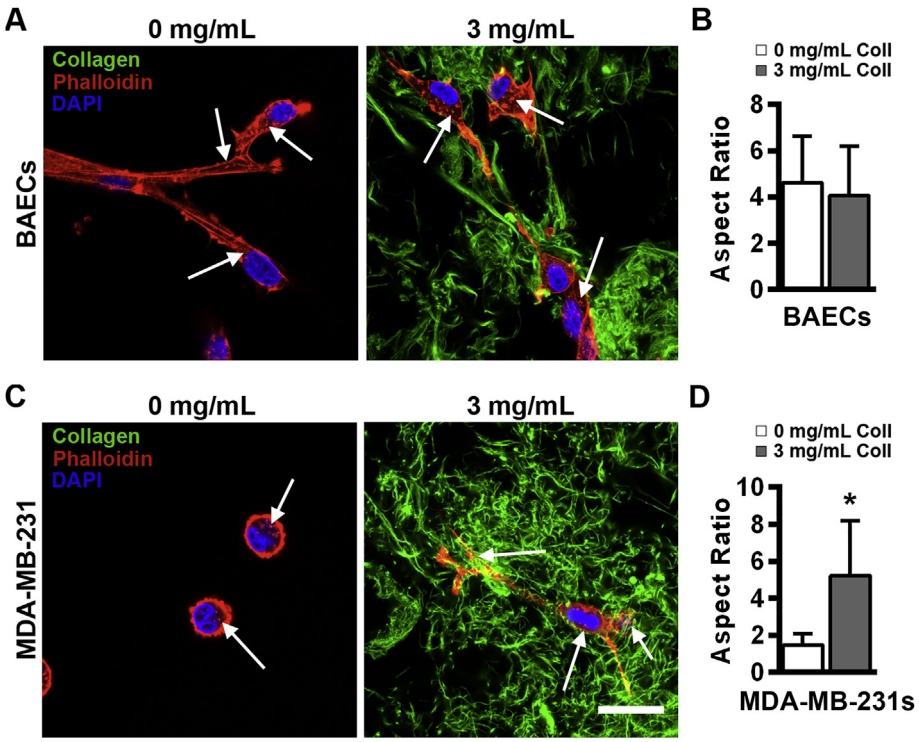

Fig. 3. Effect of collagen fibers on single-cell morphology varies with cell type. (A) BAECs exhibited a spread morphology in both the absence and presence of fibrillar collagen in 2 kPa gelMA/collagen gels. (B) The aspect ratio of cells embedded with and without collagen were similar ($p > 0.05$). $n = 16$ (C) MDA-MB-231 cells remained rounded with no significant protrusions when fibrillar collagen was not present, but elongated and adopted a spread morphology when fibers were added to the 2 kPa scaffold. (D) The addition of collagen significantly increases the observed aspect ratio of embedded cells. * indicates $p < 0.05$, $n = 22$. White arrows point to actin staining puncta. Scale bar = 25 μm. Data represent mean ± standard deviation.

stiffness of collagen gels has been manipulation of ECM concentration [19,20]. However, this approach does not allow one to discern if the effects on cell behavior are due to manipulation of stiffness, ECM fiber density, bioactive ligand density, or some combination of the three. Therefore, a key goal of this research was to develop a system that can recapitulate a wide range of physiologically relevant mechanical properties at a constant ligand density. Other collagen scaffold fabrication techniques have been developed to enable changes in mechanical properties without changing ligand density; however, the range of mechanical properties attainable with these methods is relatively small. For example, changes in polymerization pH and temperature can alter hydrogel mechanical properties, yielding 4 mg/mL collagen gels with compressive moduli from ~0.5–2 kPa [43]. Alternatively, glycation (via addition of exogenous sugars) [25] or direct acrylation of collagen [44] may be used to introduce additional cross-linking within the collagen network. However, at collagen concentrations of 1.5–2.5 mg/mL, these modifications yield only a modest range of achievable shear moduli from 0.18 to 0.5 and 0.5–1.5 kPa for glycation and acrylation, respectively. By constructing our biomaterial from the same total amount of protein but varying ratios of collagen, unmodified gelatin, and gelMA (which have the same primary sequence), we were able to successfully decouple stiffness and ligand density, while achieving a range of shear moduli (2–12 kPa) that exceeds the maximum possible in other collagen hydrogel systems. This allows for better recapitulation of a wider range of both healthy and diseased tissues *in vitro*, such as the invasive region of luminal ductal carcinoma, which has compressive moduli of up to 10 kPa [24].

This ability to decouple scaffold stiffness from total ligand density across a physiologically relevant range of stiffnesses has the potential to yield insight into cellular-microenvironmental interactions that have not been possible with existing scaffolds. In the current work, we investigated the influence of the physical cue of stiffness in the context of the tumor microenvironment by examining endothelial cell sprouting and tumor cell invasion in gelMA/collagen scaffolds. Both BAECs and MDA-MB-231 breast cancer cells have been widely utilized in studies of the impact of the physical microenvironment on cellular behavior; however, the ability to draw conclusions from these studies has been hindered by the aforementioned limitations in mechanical range and inability to separate stiffness from ligand density in existing scaffolds. In our study, both BAECs and MDA-MB-231 cells exhibited less sprouting or invasion with increases in scaffold stiffness from 2 to 12 kPa. While BAEC sprouting decreased gradually as stiffness increased, MDA-MB-231 invasion dramatically decreased when the modulus increased from 2 to 7 kPa, but was not affected by further increases in material stiffness. In contrast, prior studies of MDA-MD-231 cells and BAECs on 2D substrates demonstrated an increase in cell migration and tubulogenesis, respectively, with increased stiffness [45,46]. Others have shown that stiffer materials alter cell-generated forces [13] and adhesion preferences [47] in ECs, leading to the development of tubules, while, in MDA-MB-231 cells, a rigid substrate upregulates integrin expression, activity, and focal adhesion development [9,48]. However, it is generally appreciated that cell behavior may differ substantially between 2D and 3D environments. In 3D contexts, BAEC spheroids in glycated collagen gels (0.175–0.515 kPa) demonstrated more robust sprouting with increased stiffness [25], and a change in stiffness from 0.2 to 0.8 kPa, via collagen cross-linking with amine-reactive PEG chains, resulted in an increase in the number of MDA-MB-231 cells that migrated away from the spheroid core [49]. In contrast, our results

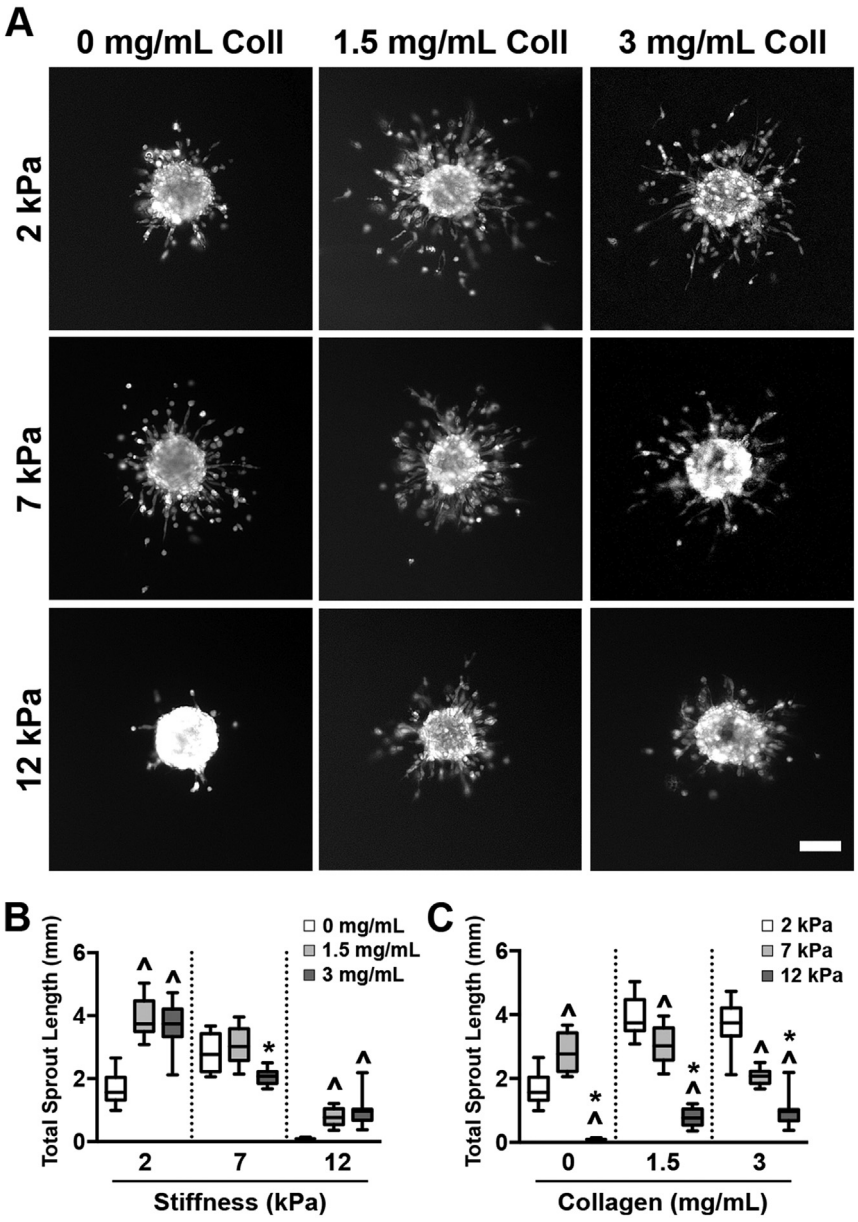

Fig. 4. The extent of BAEC sprouting from encapsulated spheroids is influenced by both collagen content and scaffold stiffness. (A) Spheroids imaged 72 h post-embedding exhibited sprouting in all scaffold conditions. Scale bar = 100 μm. (B) The addition of collagen fibers led to increased sprouting in the 2 and 12 kPa conditions, but had a minimal effect at 7 kPa ^ indicates $p < 0.01$ compared to 0 mg/mL collagen of same stiffness, * indicates $p < 0.01$ compared to 1.5 mg/mL collagen of same stiffness. n = 8–15, (C) Increased scaffold stiffness resulted in a gradual decrease in sprouting when collagen was present and a peak in sprouting at 7 kPa in non-fibrous conditions. ^ indicates $p < 0.01$ compared to 2 kPa of same collagen concentration, * indicates $p < 0.01$ compared to 7 kPa of same collagen concentration. n = 8–15. Data are presented as box and whisker plots representing the median with the 1st and 3rd quartiles (box) plus the range (whiskers).

demonstrated a general decrease in sprouting and migration with an increase in stiffness from 2 to 12 kPa, a range that better matches many native tissues. The stiffer scaffolds fabricated in this work have the potential to affect cell-generated tractional forces in a manner not observed in sub-2 kPa conditions, such as in glycated or PEG-crosslinked collagen gels.

Unlike collagen-based materials, synthetic materials, such as those based on PEG, can be tuned to a wide range of scaffold stiffnesses (<1 to >400 kPa) [29,30] while maintaining constant ligand density; however, these synthetic hydrogels lack a higher-order ECM structure. As previous studies have shown that cells are influenced by the presence of fibers [50], a second major goal of this research was to develop a material where fiber density could be manipulated. Fibers not only provide biological cues to embedded cells, but also act as a source of non-linear elasticity within the scaffold, with the capacity to uniquely influence cell-cell communication and alignment [51], as well as the degree of cell contraction [52]. Collagen-mimetic peptides that reproduce a portion of the native collagen triple helix have been incorporated into synthetic scaffolds [53,54], but these peptides cannot organize to form a fibrillar structure. Many of the collagen scaffold fabrication techniques outlined earlier may also have adverse effects on collagen fibrillogenesis and the bioactivity of the resulting fibers. For instance, altering the polymerization temperature of collagen can alter collagen fiber architecture [55], and glycation itself can be bioactive [56]. Acrylation of collagen affects the formation of the

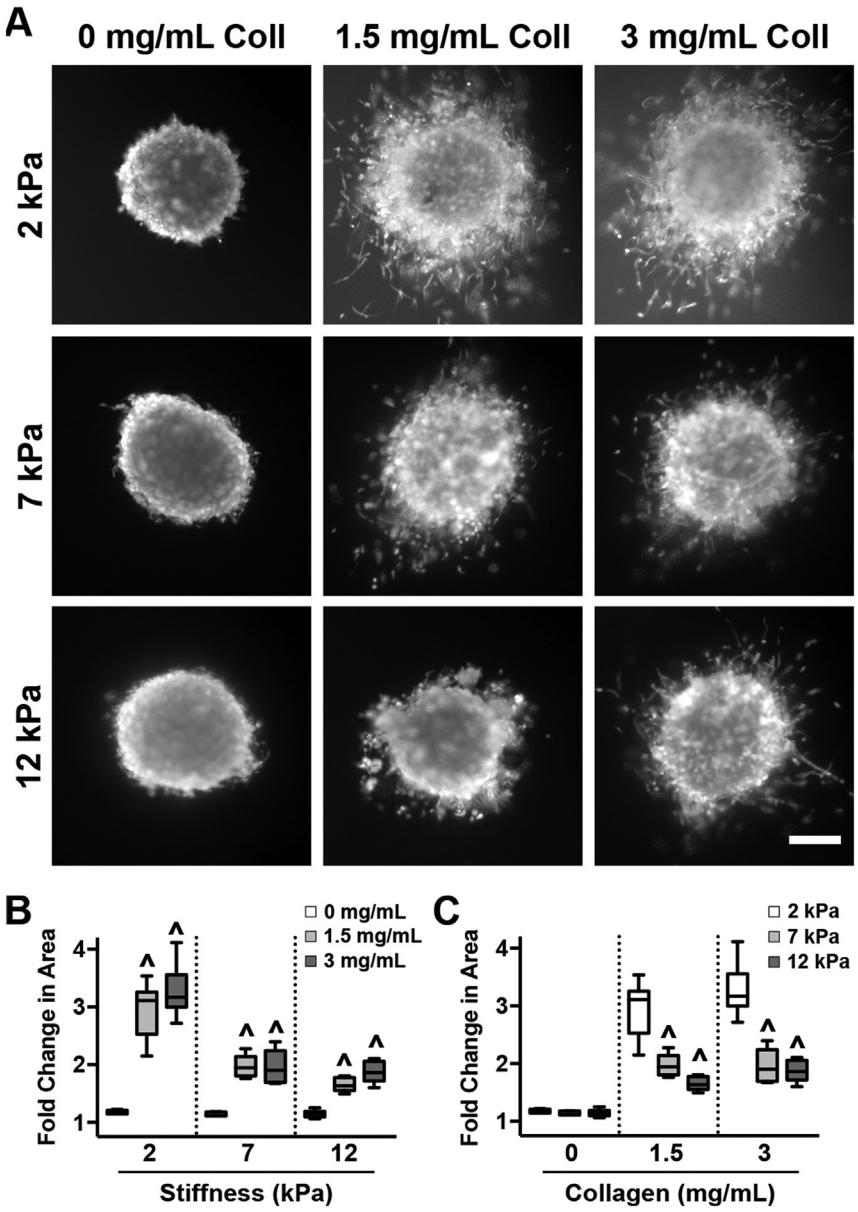

Fig. 5. MDA-MB-231 cells require fibrous collagen for invasion. (A) MDA-MB-231 spheroids were imaged 72 h after encapsulation. Scale bar = 100 μm. (B) The presence of collagen was necessary for cell invasion, but invasion was not influenced by further increases in collagen concentration. ^ indicates $p < 0.01$ to 0 mg/mL collagen of same stiffness. n = 6–9, (C) In the presence of collagen, increasing stiffness was accompanied by decreased invasion. ^ indicates $p < 0.01$ when compared to 2 kPa of same collagen concentration. n = 6–9. Data are presented as box and whisker plots representing the median with the 1st and 3rd quartiles (box) plus the range (whiskers).

collagen fibers, as demonstrated by the decrease in stiffness in non-photocrosslinked acrylated collagen gels when compared to unmodified collagen [44]. In the gelMA/collagen IPN described here, collagen fibers were preserved, and both BAECs and MDA-MB-231 cells were observed to interact with these fibers. Using our method of varying the ratio of collagen, unmodified gelatin, and gelMA, collagen fiber density could be decoupled from stiffness and total ligand density; such tuning is not possible with prior collagen-based modifications without further constraining the already limited span of achievable elastic moduli.

Changes in ECM fiber density have been suggested to play a key role in EC sprouting [57–59] and invasion of tumor cells *in vitro* [19,60,61] and *in vivo* [33,62]. In our study, the presence of collagen fibers significantly improved sprouting of ECs or invasion of MDA-MB-231 compared to gelMA alone at a given stiffness. In contrast, previous 3D research has suggested that increased ECM fiber density results in decreased EC network formation [57–59]. However, this contradiction may be due to fact that prior studies were unable to decouple the concurrent increase in scaffold rigidity and fiber density. Indeed, our results using an IPN where fiber density and stiffness are decoupled demonstrate that increased scaffold rigidity, which would be linked to increased ECM density in the above-mentioned model systems, decreases sprouting in most cases. In the range of fiber densities tested, we did not observe a concentration-dependent response to increases in collagen fiber density. However, the two cell types examined in this study showed remarkable differences in their response to an environment that lacked collagen fibers. When embedded as isolated cells in scaffolds with or without collagen fibers, both BAECs and MDA-MB-231 showed evidence of adhesion, as demonstrated by the presence

of puncta identified by f-actin staining. However, the cell types substantially differed from each other in their morphology. Specifically, BAECs exhibited a spread morphology in the absence or presence of collagen fibers. In contrast, MDA-MB-231 cells encapsulated in gelMA with 0 mg/mL collagen were unable to elongate in the absence of collagen fibers, remaining rounded with few to no protrusions. These differences in cell morphology were also reflected in the sprouting and invasion activity of BAECs and MDA-MB-231 cells. Namely, BAECs were able to sprout in the absence of fibrillar collagen, while no appreciable invasion was achieved with MDA-MB-231 cells in this condition. This finding is consistent with 2D research demonstrating that fibrillar collagen is necessary for invadopodia development in MDA-MB-231 cells [15,63]. Such differences in how individual cell types recognize their surrounding microenvironment have implications for designing scaffolds that instruct or examine cell behavior in a multi-cellular system.

5. Conclusion

Prior studies have suggested that changes in ECM density and/or stiffness impact cellular behavior; however, current model systems have been unable to distinguish between these two variables over a wide range of stiffnesses while also incorporating ECM fibers. By decoupling matrix mechanics and fiber density while maintaining equivalent total ECM quantity, the materials described herein may be used to provide insight into how these individual features of the physical microenvironment regulate cellular decision-making. Elucidating the contributions of individual microenvironmental cues to regulating cell behavior or disease pathogenesis has the potential to uncover mechanisms that may be targeted to develop new pharmacological disease treatments or achieve greater control over cell function. Additionally, examining these effects on the diverse cell types of a tissue may reveal strategies by which tissue engineers can tailor their scaffold materials to favor different outcomes for individual cell types.

Acknowledgements

This work was supported by the National Science Foundation (CBET-1401584), by the National Institutes of Health (R21CA202040 and R01GM099031), by the National Science Foundation Graduate Research Fellowship (AJB), and the Wisconsin Alumni Research Foundation (AJB). The authors gratefully acknowledge the Soft Materials Lab for support of rheometry measurements and the Optical Imaging Core for providing access to confocal microscopy.

Appendix A. Supplementary data

Supplementary data related to this article can be found at http://dx.doi.org/10.1016/j.biomaterials.2017.06.039.

References

[1] J.M. Phillip, et al., The mechanobiology of aging, Annu. Rev. Biomed. Eng. 17 (2015) 113–141.
[2] F.X. Lepelletier, et al., Early changes in extracellular matrix in Alzheimer's disease, Neuropathol. Appl. Neurobiol. 43 (2017) 167–182.
[3] A.H. Li, et al., Dynamic changes in myocardial matrix and relevance to disease: translational perspectives, Circ. Res. 114 (5) (2014) 916–927.
[4] M. Maldonado, J. Nam, The role of changes in extracellular matrix of cartilage in the presence of inflammation on the pathology of osteoarthritis, Biomed. Res. Int. (2013) 284873.
[5] D.A. Stewart, C.R. Cooper, R.A. Sikes, Changes in extracellular matrix (ECM) and ECM-associated proteins in the metastatic progression of prostate cancer, Reprod. Biol. Endocrinol. 2 (2004) 2.
[6] S.V. Plotnikov, et al., Force fluctuations within focal adhesions mediate ECM-rigidity sensing to guide directed cell migration, Cell 151 (7) (2012) 1513–1527.
[7] T. Yeung, et al., Effects of substrate stiffness on cell morphology, cytoskeletal structure, and adhesion, Cell Motil. Cytoskelet. 60 (1) (2005) 24–34.
[8] A.J. Engler, et al., Myotubes differentiate optimally on substrates with tissue-like stiffness: pathological implications for soft or stiff microenvironments, J. cell Biol. 166 (6) (2004) 877–887.
[9] M.J. Paszek, et al., Tensional homeostasis and the malignant phenotype, Cancer cell 8 (3) (2005) 241–254.
[10] P.P. Provenzano, et al., Matrix density-induced mechanoregulation of breast cell phenotype, signaling and gene expression through a FAK-ERK linkage, Oncogene 28 (49) (2009) 4326–4343.
[11] A.J. Engler, et al., Matrix elasticity directs stem cell lineage specification, Cell 126 (4) (2006) 677–689.
[12] C.M. Lo, et al., Cell movement is guided by the rigidity of the substrate, Biophys. J. 79 (1) (2000) 144–152.
[13] R.J. Pelham Jr., Y. Wang, Cell locomotion and focal adhesions are regulated by substrate flexibility, Proc. Natl. Acad. Sci. U. S. A. 94 (25) (1997) 13661–13665.
[14] R.W. Tilghman, et al., Matrix rigidity regulates cancer cell growth by modulating cellular metabolism and protein synthesis, PLoS one 7 (5) (2012) e37231.
[15] V.V. Artym, et al., Dense fibrillar collagen is a potent inducer of invadopodia via a specific signaling network, J. Cell Biol. 208 (3) (2015) 331–350.
[16] R.B. Dickinson, S. Guido, R.T. Tranquillo, Biased cell migration of fibroblasts exhibiting contact guidance in oriented collagen gels, Ann. Biomed. Eng. 22 (4) (1994) 342–356.
[17] P.P. Provenzano, et al., Engineering three-dimensional collagen matrices to provide contact guidance during 3D cell migration, Curr. Protoc. Cell Biol. 47 (2010), 10.17.1-10.17.11, (Chapter 10).
[18] K.J. Painter, Modelling cell migration strategies in the extracellular matrix, J. Math. Biol. 58 (4–5) (2009) 511–543.
[19] C.E. Barcus, et al., Stiff collagen matrices increase tumorigenic prolactin signaling in breast cancer cells, J. Biol. Chem. 288 (18) (2013) 12722–12732.
[20] E. Hadjipanayi, V. Mudera, R.A. Brown, Guiding cell migration in 3D: a collagen matrix with graded directional stiffness, Cell Motil. Cytoskelet. 66 (3) (2009) 121–128.
[21] K. Hotary, et al., A cancer cell metalloprotease triad regulates the basement membrane transmigration program, Genes & Dev. 20 (19) (2006) 2673–2686.
[22] R. Kalluri, Basement membranes: structure, assembly and role in tumour angiogenesis, Nat. Rev. Cancer 3 (6) (2003) 422–433.
[23] I. Levental, P.C. Georges, P.A. Janmey, Soft biological materials and their impact on cell function, Soft Matter 3 (2007) 299–306.
[24] I. Acerbi, et al., Human breast cancer invasion and aggression correlates with ECM stiffening and immune cell infiltration, Integr. Biol. (Camb) 7 (10) (2015) 1120–1134.
[25] B.N. Mason, et al., Tuning three-dimensional collagen matrix stiffness independently of collagen concentration modulates endothelial cell behavior, Acta Biomater. 9 (1) (2013) 4635–4644.
[26] P.F. Lee, et al., Angiogenic responses are enhanced in mechanically and microscopically characterized, microbial transglutaminase crosslinked collagen matrices with increased stiffness, Acta biomater. 9 (7) (2013) 7178–7190.
[27] Y. Liang, et al., A cell-instructive hydrogel to regulate malignancy of 3D tumor spheroids with matrix rigidity, Biomaterials 32 (35) (2011) 9308–9315.
[28] Y.C. Chen, et al., Functional human vascular network generated in photocrosslinkable gelatin methacrylate hydrogels, Adv. Funct. Mater. 22 (10) (2012) 2027–2039.
[29] K.M. Mabry, R.L. Lawrence, K.S. Anseth, Dynamic stiffening of poly(ethylene glycol)-based hydrogels to direct valvular interstitial cell phenotype in a three-dimensional environment, Biomaterials 49 (2015) 47–56.
[30] S.R. Peyton, et al., The use of poly(ethylene glycol) hydrogels to investigate the impact of ECM chemistry and mechanics on smooth muscle cells, Biomaterials 27 (28) (2006) 4881–4893.
[31] J.S. Bredfeldt, et al., Automated quantification of aligned collagen for human breast carcinoma prognosis, J. Pathol. Inf. 5 (1) (2014) 28.
[32] M.W. Conklin, et al., Aligned collagen is a prognostic signature for survival in human breast carcinoma, Am. J. Pathol. 178 (3) (2011) 1221–1232.
[33] M. Grossman, et al., Tumor cell invasion can Be blocked by modulators of collagen fibril alignment that control assembly of the extracellular matrix, Cancer Res. 76 (14) (2016) 4249–4258.
[34] D. Hanahan, R.A. Weinberg, Hallmarks of cancer: the next generation, Cell 144 (5) (2011) 646–674.
[35] D. Loessner, et al., Functionalization, preparation and use of cell-laden gelatin methacryloyl-based hydrogels as modular tissue culture platforms, Nat. Protoc. 11 (4) (2016) 727–746.
[36] B.D. Fairbanks, et al., Photoinitiated polymerization of PEG-diacrylate with lithium phenyl-2,4,6-trimethylbenzoylphosphinate: polymerization rate and cytocompatibility, Biomaterials 30 (35) (2009) 6702–6707.
[37] R.H. Ewoldt, M.T. Johnston, L.M. Caretta, Experimental Challenges of Shear Rheology: How to Avoid Bad Data. Complex Fluids in Biological Systems: Experiment, Theory, and Computation, 2015, pp. 207–241.
[38] S.J. Aper, et al., Colorful protein-based fluorescent probes for collagen imaging, PLoS One 9 (12) (2014) e114983.
[39] J. Schindelin, et al., Fiji: an open-source platform for biological-image analysis, Nat. Methods 9 (7) (2012) 676–682.
[40] I. Arganda-Carreras, et al., 3D reconstruction of histological sections: application to mammary gland tissue, Microsc. Res. Tech. 73 (11) (2010)

1019–1029.
[41] M. Heiss, et al., Endothelial cell spheroids as a versatile tool to study angiogenesis in vitro, FASEB J. 29 (7) (2015) 3076–3084.
[42] E.B. Berens, et al., A cancer cell spheroid assay to assess invasion in a 3D setting, J. Vis. Exp. (105) (2015).
[43] E.E. Antoine, P.P. Vlachos, M.N. Rylander, Tunable collagen I hydrogels for engineered physiological tissue micro-environments, PLoS One 10 (3) (2015) e0122500.
[44] I.D. Gaudet, D.I. Shreiber, Characterization of methacrylated type-I collagen as a dynamic, photoactive hydrogel, Biointerphases 7 (1–4) (2012) 25.
[45] R.W. Tilghman, et al., Matrix rigidity regulates cancer cell growth and cellular phenotype, PLoS One 5 (9) (2010).
[46] N. Yamamura, et al., Effects of the mechanical properties of collagen gel on the in vitro formation of microvessel networks by endothelial cells, Tissue Eng. 13 (7) (2007) 1443–1453.
[47] J.P. Califano, C.A. Reinhart-King, A balance of substrate mechanics and matrix chemistry regulates endothelial cell network assembly, Cell. Mol. Bioeng. 1 (2–3) (2008) 122–132.
[48] Y. Sawada, et al., Force sensing by mechanical extension of the Src family kinase substrate p130Cas, Cell 127 (5) (2006) 1015–1026.
[49] J.S. McLane, L.A. Ligon, Stiffened extracellular matrix and signaling from stromal fibroblasts via osteoprotegerin regulate tumor cell invasion in a 3-D tumor in situ model, Cancer Microenviron. 9 (2-3) (2016) 127–139.
[50] B.M. Baker, et al., Cell-mediated fibre recruitment drives extracellular matrix mechanosensing in engineered fibrillar microenvironments, Nat. Mater. 14 (12) (2015) 1262–1268.
[51] J.P. Winer, S. Oake, P.A. Janmey, Non-linear elasticity of extracellular matrices enables contractile cells to communicate local position and orientation, PLoS One 4 (7) (2009) e6382.
[52] M.S. Hall, et al., Fibrous nonlinear elasticity enables positive mechanical feedback between cells and ECMs, Proc. Natl. Acad. Sci. 113 (49) (2016) 14043–14048.
[53] S.Q. Liu, et al., Biomimetic hydrogels for chondrogenic differentiation of human mesenchymal stem cells to neocartilage, Biomaterials 31 (28) (2010) 7298–7307.
[54] A. Shekaran, et al., Bone regeneration using an alpha 2 beta 1 integrin-specific hydrogel as a BMP-2 delivery vehicle, Biomaterials 35 (21) (2014) 5453–5461.
[55] C.A. Jones, et al., The spatial-temporal characteristics of type I collagen-based extracellular matrix, Soft Matter 10 (44) (2014) 8855–8863.
[56] S.F. Kemeny, et al., Glycated collagen alters endothelial cell actin alignment and nitric oxide release in response to fluid shear stress, J. Biomech. 44 (10) (2011) 1927–1935.
[57] C.M. Ghajar, et al., The effect of matrix density on the regulation of 3-D capillary morphogenesis, Biophys. J. 94 (5) (2008) 1930–1941.
[58] L.T. Edgar, et al., Extracellular matrix density regulates the rate of neovessel growth and branching in sprouting angiogenesis, PLoS One 9 (1) (2014) e85178.
[59] A. Shamloo, S.C. Heilshorn, Matrix density mediates polarization and lumen formation of endothelial sprouts in VEGF gradients, Lab. Chip 10 (22) (2010) 3061–3068.
[60] S.P. Carey, et al., Biophysical control of invasive tumor cell behavior by extracellular matrix microarchitecture, Biomaterials 33 (16) (2012) 4157–4165.
[61] K.E. Fisher, et al., MT1-MMP- and Cdc42-dependent signaling co-regulate cell invasion and tunnel formation in 3D collagen matrices, J. Cell Sci. 122 (24) (2009) 4558–4569.
[62] P.P. Provenzano, et al., Collagen density promotes mammary tumor initiation and progression, BMC Med. 6 (2008) 11.
[63] G. Benton, et al., In vitro microtumors provide a physiologically predictive tool for breast cancer therapeutic screening, PLoS One 10 (4) (2015).